

Are ARM and TRM analogs? Thellier analysis of ARM and pseudo-Thellier analysis of TRM

Yongjae Yu*, David J. Dunlop, Özden Özdemir

Geophysics, Department of Physics, University of Toronto, Toronto, ON, Canada L5L 1C6

Received 8 August 2002; received in revised form 27 October 2002; accepted 31 October 2002

Abstract

We test the possibility of using the pseudo-Thellier method as a means of determining absolute paleointensity. Thellier analysis of anhysteretic remanent magnetization (ARM) and pseudo-Thellier analysis of thermoremanent magnetization (TRM) have been carried out on a large collection of sized synthetic magnetites and natural rocks. In all samples, the intensity of TRM is larger than that of ARM and the ratio R ($=\text{TRM}/\text{ARM}$) is strongly grain size dependent. The best-fit slope (b_{TA}) from pseudo-Thellier analysis of TRM shows a linear correlation with R . The ratio b_{TA}/R yielded approximately correct paleointensities, although uncertainties are larger than in typical Thellier-type determinations. For single-domain and multidomain magnetites, alternating field and thermal stabilities of ARM and TRM are fairly similar. However, for $\sim 0.24 \mu\text{m}$ magnetite, ARM is both much less intense and less resistant to thermal demagnetization than TRM, reflecting different domain states for the two remanences and resulting in severely non-linear Arai plots for Thellier analysis of ARM.

© 2002 Elsevier Science B.V. All rights reserved.

Keywords: TRM; ARM; Thellier method; pseudo-Thellier method; demagnetization

1. Introduction

Analog methods that substitute anhysteretic remanent magnetization (ARM) for thermoremanent magnetization (TRM) have been proposed to avoid mineralogical alteration caused by repeated heatings in Thellier-type paleointensity determina-

tion [1]. ARM techniques compare alternating field (AF) coercivity spectra rather than the unblocking temperature (T_{UB}) spectra which are compared in Thellier-type determinations. To extract relative paleointensity information from sedimentary sequences, Tauxe et al. [2] developed a pseudo-Thellier method that compares the increments of natural remanent magnetization (NRM) lost in successive AF demagnetization steps with the increments of partial ARM (pARM) acquired in the laboratory field in matching AF steps.

In rock magnetism, three aspects of the analogy

* Corresponding author. Tel.: +1-905-828-5440;
Fax: +1-905-828-3717.
E-mail address: yjyu@physics.utoronto.ca (Y. Yu).

between ARM and TRM have been examined. First, ARM and TRM have been shown to have similar AF demagnetization behavior. This similarity of ARM and TRM coercivity spectra was pointed out by Rimbert [3] and was experimentally assessed by Stephenson and Collinson [4], Levi [5], and Levi and Merrill [6,7]. In addition, this property has provided a rationale for the use of ARM instead of TRM in the Lowrie–Fuller test [8,9]. However, the similarity of T_{UB} spectra of ARM and TRM has only rarely been tested [10].

The second aspect is similarity of the applied field dependences of ARM and TRM. It has commonly been assumed that ARM and TRM intensities are proportional to field strength for weak inducing fields ($< 200 \mu\text{T}$). Thellier [11] showed experimentally that the TRM acquired by baked clays is proportional to the weak magnetic field applied during cooling. However, non-linear field dependence of TRM of fine magnetites ($0.037\text{--}0.22 \mu\text{m}$) was found in measurements with inducing fields up to 2.5 mT [12]. These same magnetites had non-linear field dependence for ARM in inducing fields up to 4 mT [13]. Non-linear TRM behavior for small equidimensional magnetites ($0.215\text{--}0.54 \mu\text{m}$) was also reported by Dunlop and Argyle [14]. A recent study using hydrothermally grown multidomain (MD) magnetite ($76 \mu\text{m}$), natural MD magnetite ($150 \mu\text{m}$), and acicular single-domain (SD) magnetite ($0.05 \mu\text{m}$) shows linearity up to $200 \mu\text{T}$ with slight non-linearity between 200 and $300 \mu\text{T}$ [15]. Thus, linearity is limited to applied fields $< 200 \mu\text{T}$.

A third aspect that requires further testing is the similarity of the grain size dependences of weak-field ARM and TRM. The ratio of ARM and TRM intensities is almost grain size independent for $> 1 \mu\text{m}$ magnetites (figure 3 of Dunlop and Argyle [14]), except for cm-size magnetite crystals [6]. However, for grains smaller than $1 \mu\text{m}$, TRM/ARM ratios are as much as an order of magnitude higher than those of $> 1 \mu\text{m}$ magnetite. This TRM/ARM peak, which is especially notable for $\sim 0.2 \mu\text{m}$ magnetite [14], has been attributed to different microstates in ARM and TRM on the basis of micromagnetic modeling [16,17]. Low ARM relative to TRM can also

be inferred from magnetic domain observations which show the nucleation of additional walls after AF demagnetization, whereas few or no domain walls existed in the TRM state [18].

In this paper, we address two questions: (1) Can we obtain accurate field intensities when we correct for the different intensities of ARM and TRM produced by the same field H ?; and (2) What is the demagnetization behavior of ARM and TRM? To answer these questions, we apply the pseudo-Thellier method to TRM and the Thellier technique to ARM and compare these results with the results of pseudo-Thellier analysis of ARM and Thellier analysis of TRM. The results of using the pseudo-Thellier method on TRM are of practical interest since the Thellier method is very time-consuming and has a low success rate.

2. Samples and experimental procedures

2.1. Samples

Eight synthetic samples were prepared using magnetite powders whose mean grain sizes range from single-domain (SD, $0.065 \mu\text{m}$) to small multidomain (MD, $18.3 \mu\text{m}$) [19]. Grain sizes were determined using a Hitachi S-4500 scanning electron microscope. These samples are 0.5% by volume dispersions of magnetite in a matrix of CaF_2 . Cylindrical pellets 8.8 mm in diameter and 8.6 mm in height were pressed and then tightly wrapped with quartz wool inside quartz capsules. The capsules were sealed under vacuum and annealed for 3 h at 700°C to stabilize the magnetic properties [7,14].

Seventeen natural samples were also studied: two andesites (An 1, An 3) and one red-scoria (Km 3) [20], 11 gabbros [21,22], and three granites [23,24]. The natural samples selected have magnetic and paleomagnetic properties that are well documented. They were chosen from a much larger collection of several hundred cores on the basis of their low magnetic fabric anisotropy, their reproducible ARM and TRM intensities, and minimal viscous magnetic changes. In addition, the gabbros had yielded reliable paleointensities

from Thellier analyses. Samples were cylindrical, 2.3 cm in diameter and 2.0 cm in height.

2.2. Experiments

2.2.1. Pseudo-Thellier analyses of TRM

After thermal demagnetization, a total TRM was produced by cooling from 600°C in a laboratory field $H = 50 \mu\text{T}$. Stepwise AF demagnetization was performed with a step increment of 5 mT. Double demagnetization [2] was carried out along three orthogonal axes (x, y, z) followed by a remanence measurement, then demagnetization along $(-x, -y, -z)$, and finally a second remanence measurement. Partial ARM (pARM) was then produced at the same AF level in a steady field of 50 μT . TRM lost was plotted against pARM gained at each AF step in the style of an Arai plot [25].

2.2.2. Thellier analyses of ARM

After thermal demagnetization to 600°C, ARM was imparted along z in an AF decaying from 100 mT with a superimposed steady field $H = 50 \mu\text{T}$.

The Coe-modified Thellier method [26] was then applied. After the first (zero-field) heating-cooling step to temperature T_i , the remanence was measured and the ‘NRM’ (i.e. ARM) lost was calculated. The second heating-cooling step to temperature T_i was in $H = 50 \mu\text{T}$ along the cylindrical z axis of the specimen. Subtraction of the first- and second-step remanences gave the partial TRM (pTRM) acquired at T_i . Double heatings were carried out at 250, 300, 350, 400, 450, 480, 510, 530, 550, 565, 575, and 580°C using an MMTD (Shaw) furnace. We made pTRM checks at 250, 350, 450, 510, 550, and 575°C. Throughout all heat treatments, temperatures were reproducible within $\pm 2^\circ\text{C}$. The residual field in the furnace during heatings and coolings was less than 150 nT.

2.2.3. Pseudo-Thellier analyses of ARM and Thellier analyses of TRM

For comparison, pseudo-Thellier analyses of ARM and Thellier experiments on TRM were carried out using exactly the same (or the exact same) experimental procedures described above.

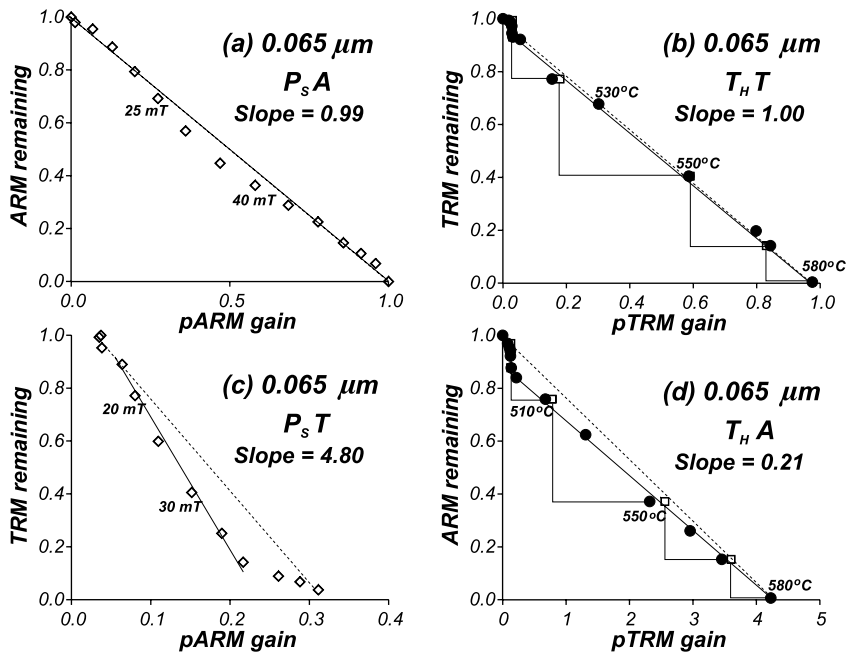


Fig. 1. Experimental results of (a) P_sA (=pseudo-Thellier analysis of ARM), (b) $T_H T$ (=Thellier analysis of TRM), (c) $P_s T$ (=Pseudo-Thellier analysis of TRM), and (d) $T_H A$ (=Thellier analysis of ARM) for the 0.065 μm SD magnetite sample.

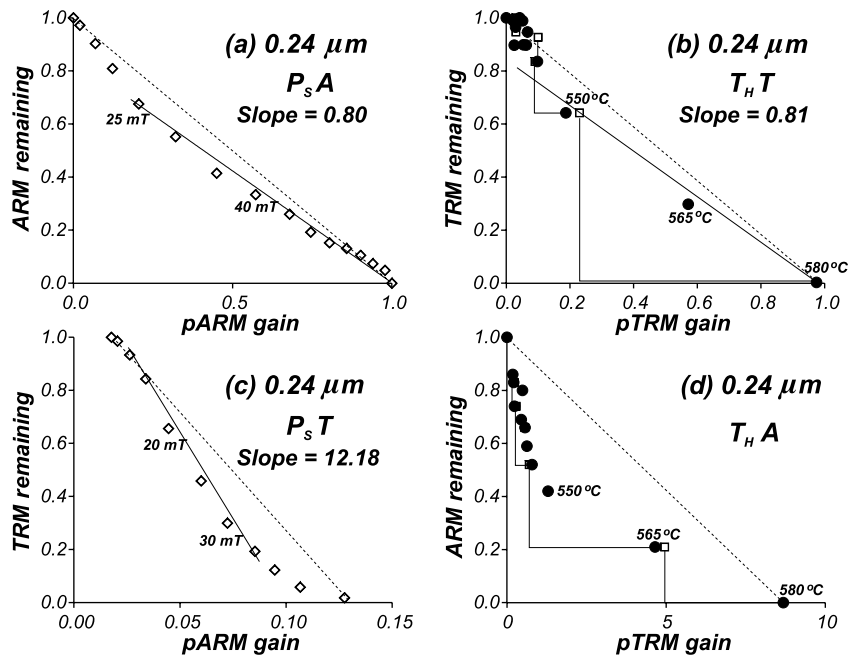


Fig. 2. Arai plots of (a) $P_S A$, (b) $T_H T$, (c) $P_S T$, and (d) $T_H A$ experiments for the $0.24 \mu\text{m}$ magnetite sample.

For convenience, Thellier analyses of ARM, pseudo-Thellier analyses of TRM, pseudo-Thellier analyses of ARM, and Thellier analyses of TRM will be denoted as $T_H A$ (=Thellier ARM), $P_S T$ (=pseudo-Thellier TRM), $P_S A$ (=pseudo-Thellier ARM), and $T_H T$ (=Thellier TRM), respectively.

A Molspin AF demagnetizer was used for AF demagnetization and for pARM acquisition. Remanences were measured with a Minispin magnetometer. All the synthetic samples were heated in air and the natural samples in argon. To monitor possible chemical alteration, bulk magnetic susceptibility was measured after every heating. All the samples showed less than 2% overall change of bulk susceptibility throughout all heatings, implying that alteration was minimal.

3. Results

3.1. Synthetic samples

Typical results for $P_S T$, $T_H A$, $P_S A$, and $T_H T$ experiments are presented in Figs. 1–3. All inten-

sities are normalized to the initial ARM for $T_H A$ and $P_S A$ and to the initial TRM for $P_S T$ and $T_H T$. For comparison, the ideal lines connecting corresponding total ARMs and/or TRMs are shown (dotted lines). The best-fit (solid) lines were calculated to minimize the quality factor (S') values. S' [27] represents the quality of least-squares fitting more precisely than the conventional quality factor q [28]. Both q and S' are given in Table 1.

For synthetic SD magnetite ($0.065 \mu\text{m}$), $T_H T$ yielded almost a perfect fit, following the ideal SD line (Fig. 1b). $P_S A$ was slightly non-linear (Fig. 1a), suggesting that AF demagnetization and ARM are not reciprocal processes [29]. More strongly convex-down shapes of the Arai plots were observed for $P_S T$ and $T_H A$ analyses, leading to overestimation or underestimation of the slopes (Fig. 1c,d). The $T_H A$ and $P_S T$ slopes are reciprocal, indicating $T_H A$ and $P_S T$ analyses may be used for SD samples if the difference in ARM and TRM intensities can be adequately compensated.

The $P_S A$ and $T_H T$ analyses for synthetic pseudo-single-domain (PSD) magnetite ($0.24 \mu\text{m}$)

show that it was easier to AF or thermally demagnetize a remanence in the first step (zero-field step) than to restore the same remanence in the second step (in-field step) (Fig. 2a,b). As a result, the Arai plots are non-linear and paleointensities are underestimated by $\sim 20\%$ if determined from high coercivity or T_{UB} points. If low coercivity or T_{UB} points are used, paleointensities are overestimated. In Fig. 2c, the large slope of the ideal line in $P_S T$ analysis results from the peak TRM/ARM ratio around $\sim 0.2 \mu\text{m}$ (figure 3 of Dunlop and Argyle [14]). T_{HA} yielded severely non-linear Arai plots (Fig. 2d).

Synthetic MD samples yielded convex-down non-linear Arai plots regardless of the experimental scheme used (Fig. 3). Consequently, no acceptable slopes could be calculated.

3.2. Natural samples

Among the 17 natural samples studied, three representative examples are illustrated in Figs. 4–6. T 19 (Tudor Gabbro, Madoc, ON, Canada) yielded a reliable Thellier result in a previous study [21]. The interesting characteristic of T 19

is that the Thellier analyses (Fig. 4b,d) yielded better fits than the pseudo-Thellier analyses (Fig. 4a,c). For example, $P_S A$ gave a 19% overestimation (Fig. 4a) while T_{HT} overestimated by only 4% (Fig. 4b). The T_{HA} analyses also follow the ideal SD line (Fig. 4d) but $P_S T$ yielded rather curved results (Fig. 4c). Interestingly, the estimated slopes for T_{HA} and $P_S T$ analyses are almost reciprocal (Fig. 4c,d), as for the synthetic SD magnetite, indicating that the magnetic carriers in T 19 are nearly SD magnetite (see also Figs. 7d and 8d).

For An 1 (An-ei Andesite, Mt. Sakurajima, Japan), the T_{HT} and $P_S A$ analyses paralleled the ideal SD line, yielding accurate paleointensities (Fig. 5a,b). The $P_S T$ data also show a good linear relationship between TRM remaining and pARM acquisition (Fig. 5c). However, T_{HA} analyses yielded a convex-down Arai plot that is not seen in $P_S A$, $P_S T$, or T_{HT} analyses (Fig. 5d).

It was anticipated that Bu 5 (Burchell Lake Granite, Shebandowan, ON, Canada) would mimic the properties of the synthetic MD sample ($18.3 \mu\text{m}$) since the inferred domain state of Bu 5 from the Day plot [30] and from demagnetization

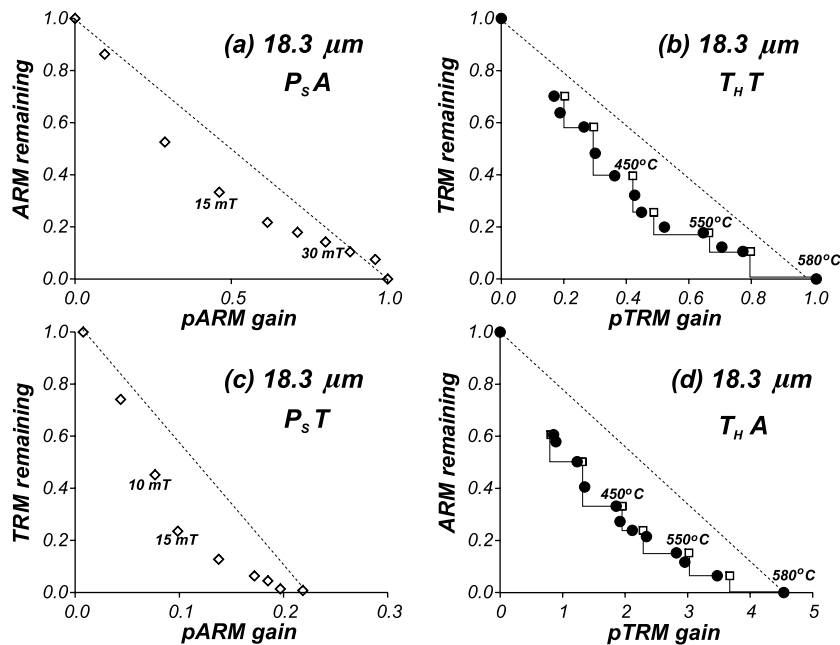


Fig. 3. Intensity determinations on Arai plots for MD magnetite ($18.3 \mu\text{m}$) $P_S A$ (a), T_{HT} (b), $P_S T$ (c), and T_{HA} (d) analyses.

properties was coarse PSD to MD [19]. T_{HA} and P_{ST} experiments did yield MD-style Arai plots, but P_{SA} and T_{HT} analyses actually yielded relatively linear trends in their Arai plots (Fig. 6).

4. Discussion

4.1. Demagnetization behavior

The main question we wish to answer in this paper is, ‘Can P_{ST} analysis yield reliable paleointensities if a correction factor allowing for the different acquisition capacities of ARM and TRM is applied?’ Answering this question is of practical importance because P_{ST} analyses are much easier and faster than T_{HT} analyses.

Physically the demagnetization behavior of ARM and TRM can be quite different (Figs. 7 and 8). However, for synthetic samples, there is little difference between AF demagnetization

curves for ARM and TRM, except that TRM is harder (more resistant to demagnetization) than ARM at higher AF steps for SD and PSD samples as compared to MD samples (Fig. 7a–c). This harder TRM at higher coercivities causes kinks in P_{ST} analyses for SD and PSD samples (Figs. 1c and 2c). Dual segments on Arai plots are generally attributed to MD behavior. However, at least for the synthetic samples used in this study, the dual segments in Figs. 1c and 2c are caused by the different coercivity spectra of ARM and TRM above 20–30 mT.

Thermal demagnetization curves of ARM and TRM are virtually indistinguishable for SD and MD grains (Fig. 7d,f), but TRM is decisively harder than ARM for 0.24 μm PSD grains (Fig. 7e). For PSD grains, it is quite striking that the ARM shows distributed T_{UB} spectra (MD characteristics [31]) while TRM has the SD-like property of discrete high T_{UB} s. As a result, T_{HA} analyses yielded severely non-linear Arai plots for PSD grains (Fig. 2d). This further evidence of a difference in domain state between ARM and TRM for $\sim 0.24 \mu\text{m}$ magnetite is consistent with the interpretation in Section 1 based on the peak in the TRM/ARM ratio around this grain size.

The results for the natural samples confirm the explanation provided for the synthetic samples. For T 19 and An 1, TRM is harder than ARM for corresponding AF steps (Fig. 8a,b). This is mainly because an AF of 100 mT is not enough to erase TRM in natural samples. In thermal demagnetizations, TRM is harder than ARM for An 1, while T 19 and Bu 5 show fairly similar demagnetization properties of ARM and TRM (Fig. 8d–f).

Another interesting point worthy of note is that best-fit slopes of P_{ST} and T_{HA} Arai plots are reciprocal only for SD grains. The different thermal stabilities of ARM and TRM are responsible for non-reciprocal slopes in T_{HA} and P_{ST} experiments for PSD grains. For MD samples, convex-down non-linear Arai plots prevent reasonable slope calculations although the AF and thermal stabilities of ARM and TRM are similar.

Overall, AF and thermal demagnetization of ARM and TRM show the following properties:

Table 1
Experimental estimation of H^a

Sample	b_{TA}	R	H	q	S'
Ideal			1		
0.065 μm	4.80	4.23	1.14	22.07	0.90
0.21 μm	9.17	7.21	1.27	17.60	1.66
0.44 μm	6.21	4.80	1.30	15.33	1.33
0.24 μm	12.18	8.68	1.40	16.79	1.36
0.34 μm	6.48	5.54	1.17	16.29	0.92
1.06 μm	5.20	5.17	1.01	17.37	0.63
An 1	2.34	3.40	0.69	10.70	0.65
An 3	2.31	3.36	0.69	25.60	0.84
C 12	2.89	3.15	0.92	20.39	0.65
C6 A2	2.91	3.36	0.87	20.53	0.50
C6 B1	2.77	2.74	1.01	22.74	0.62
C6 C1	3.17	3.73	0.85	24.57	0.71
Km 3	9.53	11.04	0.86	15.40	0.76
T1 A1	2.67	2.52	1.06	21.75	0.55
T1 A2	3.04	2.59	1.18	22.38	0.98
T1 C1	3.00	2.79	1.08	22.54	0.67
T1 F1	2.79	2.70	1.03	18.76	0.73
T1 G1	2.78	2.42	1.15	20.69	0.51
T2 B1	3.12	2.34	1.34	18.00	0.56
T 19	7.24	8.20	0.88	22.70	0.42
Mean			1.04		
σ			0.20		

^a b_{TA} , best-fit slopes of P_{ST} analyses; R , TRM/ARM ratio; $H = b_{TA}/R$; σ , standard deviation; q [28] and S' [27] are quality factors; actual (normalized) value of H is 1 in all cases.

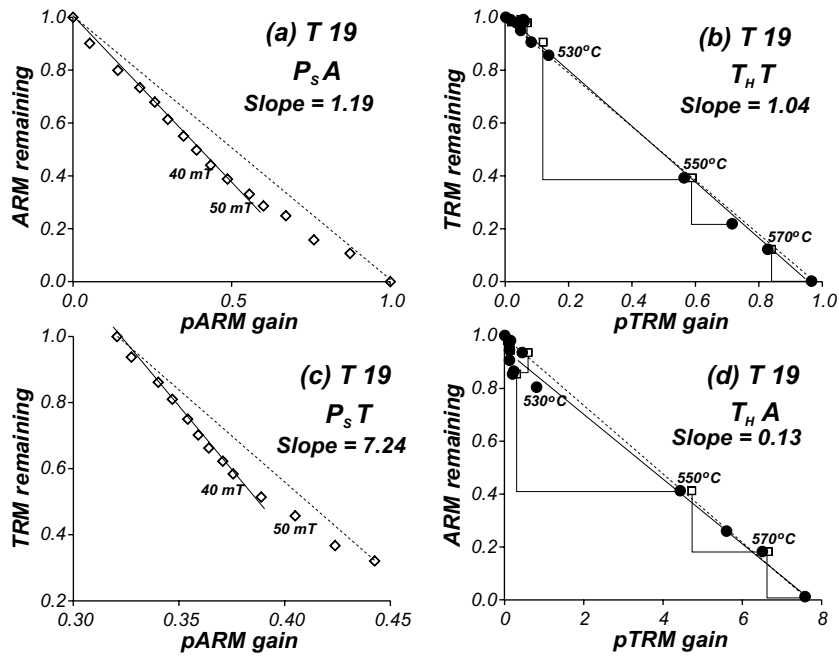


Fig. 4. Results of $P_s A$ (a), $T_H T$ (b), $P_s T$ (c), and $T_H A$ (d) experiments for Tudor Gabbro sample T 19.

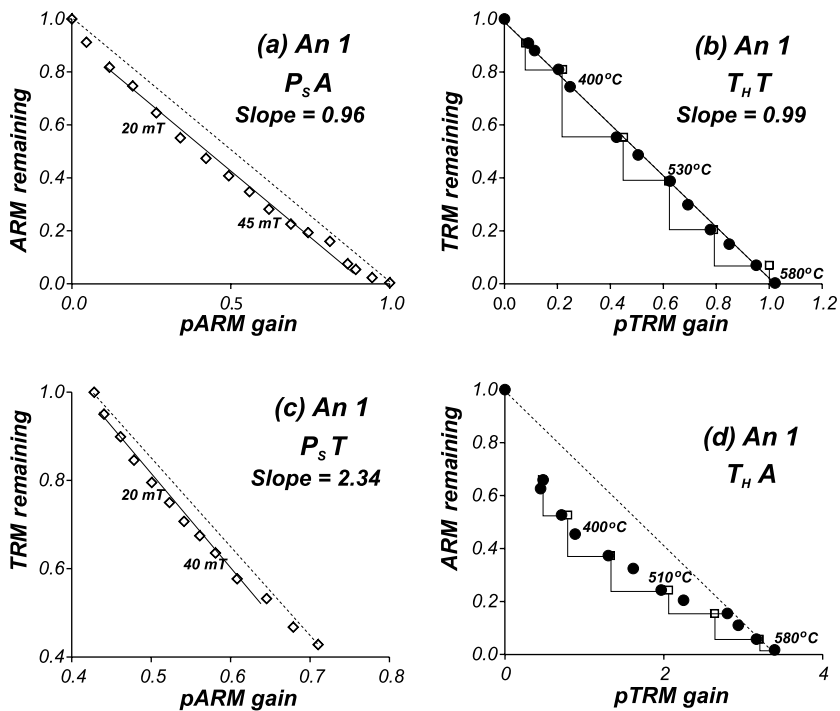


Fig. 5. Results of $P_s A$ (a), $T_H T$ (b), $P_s T$ (c), and $T_H A$ (d) experiments for An-ei Andesite sample An 1.

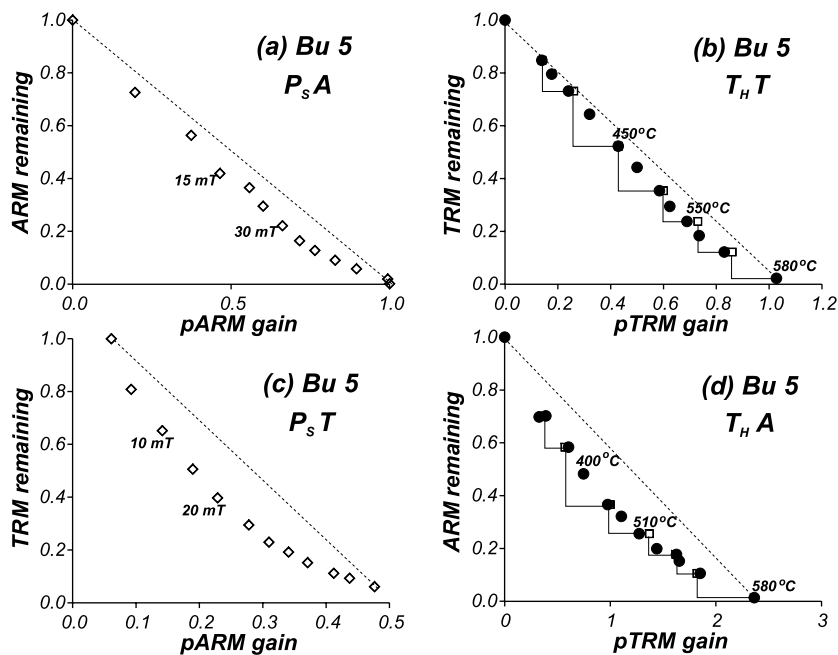


Fig. 6. (a) $P_S A$, (b) $T_H T$, (c) $P_S T$, and (d) $T_H A$ analyses for Burchell Lake Granite sample Bu 5.

1. Thermal demagnetizations of ARM and TRM are obviously different for PSD magnetites. ARM is much softer (less resistant to demagnetization) than TRM, resulting in very non-linear T_{HA} analyses (Figs. 2d and 5d). This interesting feature likely originates from different microstates for ARM and TRM. Significantly different demagnetization stability, AF as well as thermal, seems to be inherited from fundamentally different domain states in ARM and TRM. For $\sim 0.2 \mu\text{m}$ magnetite, SD or two-domain (2D) states were inferred for TRM whereas a vortex state was attributed to ARM [14]. Possibly the vortex state is less resistant to thermal demagnetization than SD or 2D states.
2. AF demagnetization curves of ARM and TRM are quite similar but TRM is a little harder than ARM for SD/PSD grains, particularly at higher coercivities.

Previous studies comparing AF coercivities of ARM and TRM have found results similar to (2) [3–9,32]. Dunlop and West [10] found trends similar to (1) and (2) for ARM and TRM of SD grains.

4.2. Correlation between b_{TA} and R

Neither $P_S T$ nor T_{HA} analyses yielded a slope of 1. This is natural since ARM and TRM have different capacities or efficiencies in acquiring remanence. Then how well does b_{TA} (the best-fit slope in $P_S T$ analyses) correlate with the ratio R (=total TRM/total ARM)? These two values should be identical in the ideal case since TRM is progressively replaced by ARM in $P_S T$ analyses.

For the synthetic samples, values of b_{TA} are plotted as a function of grain size in Fig. 9a. Best fits were unavailable for the MD synthetic samples because of their non-linear behavior in the Arai plots (e.g. Fig. 3c). The slopes from $P_S T$ analyses are compared to the R ratio in Fig. 9b for both synthetic and natural samples. The two parameters show a rough linear correlation as expected. The R ratio was deduced not by the end data points in either $P_S T$ or T_{HA} analyses but by separate experimental determinations that used thermally demagnetized initial states. Fig. 9a has a strong peak at $\sim 0.2 \mu\text{m}$, agreeing well with the compiled R ratios in figure 3 of Dunlop and Argyle [14]. It is interesting that synthetic samples

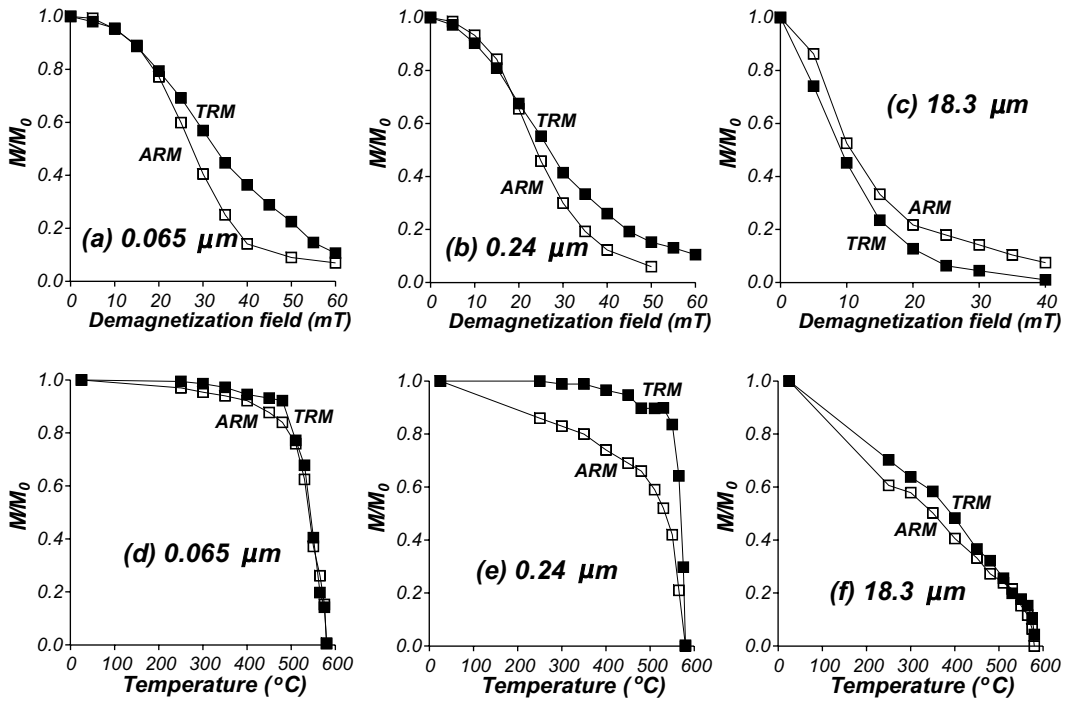


Fig. 7. AF and thermal demagnetization of ARM and TRM for 0.065 μm (a,d), 0.24 μm (b,e), and 18.3 μm (c,f) magnetite samples.

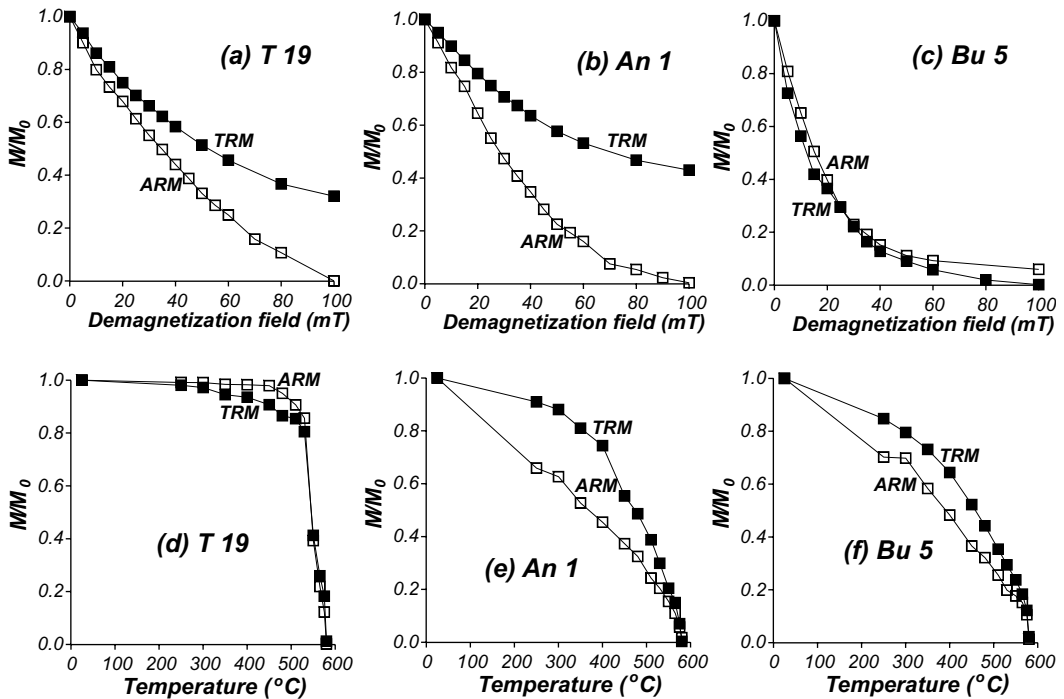


Fig. 8. Comparison of AF and thermal stabilities of ARM and TRM for natural samples T 19 (a,d), An 1 (b,e), and Bu 5 (c,f).

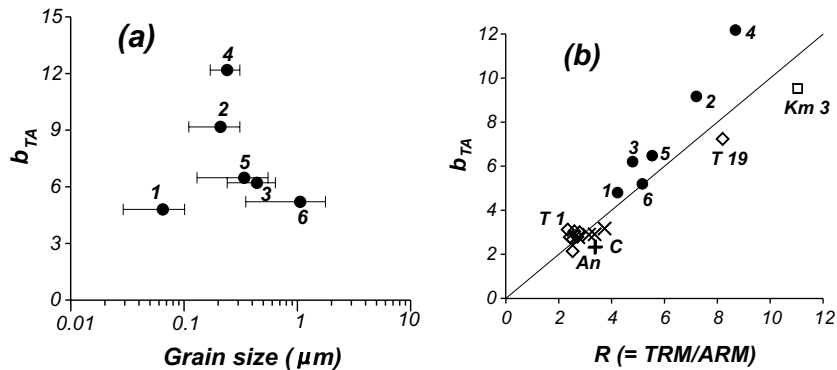


Fig. 9. (a) Estimated slopes from pseudo-Thellier analyses of TRM ($=b_{TA}$) as a function of grain size. (b) Correlation between b_{TA} and $R (= \text{TRM}/\text{ARM}$ ratio). The line is a 1–1 relation, $b_{TA} = R$. Synthetic samples (solid circles): 1, 0.065 μm ; 2, 0.21 μm ; 3, 0.44 μm ; 4, 0.24 μm ; 5, 0.34 μm ; 6, 1.06 μm ; An, An-ei basalts (plusses) [17]; Km 3, Kometsuka red-scoria (square) [17]; T, Tudor Gabbro (diamonds) [18]; C, Cordova Gabbro (crosses) [19].

follow a line of steeper slope than the natural samples (Fig. 9).

4.3. Practical use of $P_S T$ analyses

According to the results in the previous section, practical application of $P_S T$ (pseudo-Thellier analysis of TRM) seems possible in some cases. Using b_{TA} by itself is not possible since b_{TA} has a strong grain size dependence (Fig. 9a). High values of b_{TA} do not necessarily indicate high paleointensities (e.g. Table 1).

In practice, in order to estimate the correct paleointensity, b_{TA} (best-fit slope of the $P_S T$ Arai plot) is divided by the measured ratio R for a particular sample. This process is similar in principle to the Shaw method [33]. This equality of b_{TA} and R is tested directly in the $P_S T$ analysis but is implicitly assumed in the Shaw method.

The correlation of b_{TA} with the measured R value ideally gives $H = b_{TA}/R = 1$ since the $P_S T$ Arai plots were normalized to initial TRM. Values of H calculated for the present samples (Table 1) are quite encouraging, in that the mean value of H is 1.04. In other words, $P_S T$ analyses are potentially usable in order to estimate absolute paleointensity values. However, although the mean value is fairly close to the ideal value of 1, some results overestimate or underestimate the field by 30% or more and exceed acceptable error

limits in Thellier-type paleointensity determination. Therefore, $P_S T$ analyses are worthwhile, but only as a supplementary tool.

According to Table 1, estimating H by $P_S T$ analysis gives a useful approximate paleointensity value, particularly when chemical alteration is unavoidable, e.g. in many volcanic rocks. A similar approach has recently been put into practice by carrying out pseudo-Thellier paleointensity determinations for Icelandic lavas from Chron C5N in an attempt to minimize the effect of alteration [34]. Correction of the $P_S T$ results to obtain absolute paleointensities was not attempted, but paleointensities from the pseudo-Thellier analyses were linearly correlated with those from Thellier determinations [34].

4.4. Why does $P_S T$ work while T_{HA} fails?

Experimental results clearly demonstrate (Figs. 1–6) that $P_S T$ analysis (i.e. the pseudo-Thellier method) is a viable method of estimating approximate absolute paleointensities, while T_{HA} analysis fails. The substantial non-linearity in T_{HA} analyses results from the different thermal demagnetization behavior of ARM and TRM (Figs. 7 and 8). On the other hand, $P_S T$ analyses for synthetic samples were quite successful because ARM and TRM have fairly similar AF demagnetization behavior (Figs. 7 and 8).

5. Conclusions

1. In this study, TRM was always more intense than ARM.
2. The ratio R ($= \text{TRM}/\text{ARM}$) has a strong grain size dependence. The ratio R also shows a linear correlation with the best-fit slope (b_{TA}) from pseudo-Thellier analysis of TRM.
3. The pseudo-Thellier method provides reliable absolute intensities when the difference in acquisition efficiencies of ARM and TRM is properly compensated, although uncertainties are larger than in typical Thellier-type determinations.
4. Very different thermal stabilities of ARM and TRM for PSD grains result in severely non-linear Arai plots for Thellier analysis of ARM.
5. For 0.24 μm magnetite, ARM and TRM domain states are different, based on both R values and thermal demagnetization results.

Acknowledgements

We wish to thank Shaul Levi and John Shaw for helpful comments and Nancy Bowers for significant improvements to the manuscript. This research has been supported by the Natural Sciences and Engineering Research Council of Canada through Grant A7709 to D.J.D. [RV]

References

- [1] E. Thellier, O. Thellier, Sur l'intensité du champ magnétique terrestre dans le passé historique et géologique, *Ann. Geophys.* 15 (1959) 285–376.
- [2] L. Tauxe, T. Pick, Y.S. Kok, Relative paleointensity in sediments: a pseudo-Thellier approach, *Geophys. Res. Lett.* 22 (1995) 2885–2888.
- [3] F. Rimbart, Contribution à l'étude de l'action de champs alternatifs sur les aimantations rémanentes des roches. Applications géophysiques, *Rev. Inst. Fr. Pétrole* 14 (1959) 17–54 and 123–155.
- [4] A. Stephenson, D.W. Collinson, Lunar magnetic field paleointensities determined by an anhysteretic remanent magnetization method, *Earth Planet. Sci. Lett.* 23 (1974) 220–228.
- [5] S. Levi, Some magnetic properties of magnetite as a function of grain size and their implications for paleomagnetism, Ph.D. Thesis, Univ. of Washington, Seattle, WA, 1974, 210 pp.
- [6] S. Levi, R.T. Merrill, A comparison of ARM and TRM in magnetite, *Earth Planet. Sci. Lett.* 32 (1976) 171–184.
- [7] S. Levi, R.T. Merrill, Properties of single-domain, pseudo-single-domain, and multidomain magnetite, *J. Geophys. Res.* 83 (1978) 309–323.
- [8] W. Lowrie, M. Fuller, On the alternating field demagnetization characteristics of multidomain thermoremanent magnetization in magnetite, *J. Geophys. Res.* 76 (1971) 6339–6349.
- [9] H.P. Johnson, W. Lowrie, D.V. Kent, Stability of anhysteretic remanent magnetization in fine and coarse magnetite and maghemite particles, *Geophys. J. R. Astron. Soc.* 41 (1975) 1–10.
- [10] D.J. Dunlop, G.F. West, An experimental evaluation of single domain theories, *Rev. Geophys.* 7 (1969) 709–757.
- [11] E. Thellier, Sur l'aimantation des terres cuites et ses applications géophysiques, *Ann. Inst. Phys. Globe Univ. Paris Bur.* 16 (1938) 157–302.
- [12] D.J. Dunlop, F.D. Stacey, D.E.W. Gillingham, The origin of thermoremanent magnetization: contribution of pseudo-single-domain magnetite moments, *Earth Planet. Sci. Lett.* 21 (1974) 288–294.
- [13] D.J. Dunlop, Grain size dependence of anhysteresis in iron oxide micropowders, *IEEE Trans. Magn.* 8 (1972) 211–213.
- [14] D.J. Dunlop, K.S. Argyle, Thermoremanence, anhysteretic remanence and susceptibility of submicron magnetites: Nonlinear field dependence and variation with grain size, *J. Geophys. Res.* 102 (1997) 20,199–20,210.
- [15] A.R. Muxworthy, E. McClelland, The causes of low-temperature demagnetization of remanence in multidomain magnetite, *Geophys. J. Int.* 140 (2000) 115–131.
- [16] L.C. Thompson, R.J. Enkin, W. Williams, Simulated annealing of three-dimensional micromagnetic structures and simulated thermoremanent magnetization, *J. Geophys. Res.* 99 (1994) 603–609.
- [17] W. Williams, D.J. Dunlop, Simulation of magnetic hysteresis in pseudo-single-domain grains of magnetite, *J. Geophys. Res.* 100 (1995) 3859–3871.
- [18] S.L. Halgedahl, Magnetic domain patterns observed on synthetic Ti-rich titanomagnetite as a function of temperature and in states of thermoremanent magnetization, *J. Geophys. Res.* 96 (1991) 3943–3972.
- [19] Y. Yu, D.J. Dunlop, Ö. Özdemir, Partial anhysteretic remanent magnetization in magnetite 1. Additivity, *J. Geophys. Res.* B 107 (2002) 10.1029/2001JB001249.
- [20] Y. Yu, Rock magnetic and paleomagnetic experiments on hemoilmenites and titanomagnetites in some volcanic rocks from Japan, M.Sc. Thesis, University of Toronto, 1998, p. 24.
- [21] Y. Yu, D.J. Dunlop, Paleointensity determination on the late Precambrian Tudor Gabbro, Ontario, *J. Geophys. Res.* 106 (2001) 26,331–26,344.
- [22] Y. Yu, D.J. Dunlop, Multivectorial paleointensity deter-

- mination from the Cordova Gabbro, southern Ontario, *Earth Planet. Sci. Lett.* 203 (2002) 983–998.
- [23] D.J. Dunlop, Paleomagnetism of Archean rocks from northwestern Ontario: 4. Burchell Lake granite, Wawa-Shebandowan Subprovince, *Can. J. Earth Sci.* 21 (1984) 1098–1104.
- [24] D.J. Dunlop, L.D. Schutts, C.J. Hale, Paleomagnetism of Archean rocks from northwestern Ontario: 3. Rock magnetism of the Shelley Lake granite, Quetico Subprovince, *Can. J. Earth Sci.* 21 (1984) 879–886.
- [25] T. Nagata, Y. Arai, K. Momose, Secular variation of the geomagnetic total force during the last 5000 years, *J. Geophys. Res.* 68 (1963) 5277–5281.
- [26] R.S. Coe, Paleointensities of the Earth's magnetic field determined from Tertiary and Quaternary rocks, *J. Geophys. Res.* 72 (1967) 3247–3262.
- [27] Y. Yu, D.J. Dunlop, L. Pavlish, M. Cooper, Archeomagnetism of Ontario potsherds from the last 2000 years, *J. Geophys. Res.* 105 (2000) 19,419–19,433.
- [28] R.S. Coe, C.S. Grommé, E.A. Mankinen, Geomagnetic paleointensities from radiocarbon-dated lava flows on Hawaii and the question of the Pacific nondipole low, *J. Geophys. Res.* 83 (1978) 1740–1756.
- [29] Y. Yu, D.J. Dunlop, Ö. Özdemir, Partial anhysteretic remanent magnetization in magnetite 2. Reciprocity, *J. Geophys. Res. B* 107 (2002) 10.1029/2001JB001269.
- [30] R. Day, M. Fuller, V.A. Schmidt, Hysteresis properties of titanomagnetites: Grain-size and compositional dependence, *Phys. Earth Planet. Inter.* 13 (1977) 260–267.
- [31] D.J. Dunlop, Ö. Özdemir, *Rock Magnetism: Fundamentals and Frontiers*, Cambridge Univ. Press, New York, 1997, 573 pp.
- [32] D.J. Dunlop, J.A. Hanes, K.L. Buchan, Indices of multidomain magnetic behavior in basic igneous rocks: alternating-field demagnetization, hysteresis, and oxide petrology, *J. Geophys. Res.* 102 (1973) 27,285–27,295.
- [33] J. Shaw, A new method of determining the magnitude of the paleomagnetic field, *Geophys. J.* 39 (1974) 133–141.
- [34] J.S. Gee, S. Cande, N. Bowers, Relative paleointensity variations in Icelandic lavas from chron C5N (abstract), *EOS Trans. AGU* 82 (2001) F344.